Environmental Science Processes & Impacts

PAPER

View Article Online
View Journal | View Issue

Cite this: *Environ. Sci.: Processes Impacts*, 2025, **27**, 2755

Controls on the apparent quantum yield for photomineralization of dissolved organic matter in arctic freshwaters

Emma C. Rieb, †[a] Catherine A. Polik, ‡[a] George W. Kling [b] and Rose M. Cory *[a]

The oxidation of dissolved organic matter (DOM) to carbon dioxide by sunlight (photomineralization) can account for up to 30% of carbon dioxide (CO_2) emitted from inland surface waters in the Arctic. Water-column photomineralization rates depend on the magnitude and shape of the photomineralization apparent quantum yield spectrum ($\varphi_{PM,\lambda}$), which few studies have quantified directly. Here, we used a light-emitting diode (LED)-based approach to directly quantify $\varphi_{PM,\lambda}$ of CO_2 from photomineralization in arctic surface waters exposed to increasing amounts of narrow-banded light at ultraviolet and visible wavelengths. Waters with the highest aromatic DOM and dissolved iron had the highest $\varphi_{PM,\lambda}$ at all wavelengths. The magnitude of $\varphi_{PM,\lambda}$ at all wavelengths decreased by up to 92% with increasing cumulative light absorbed by chromophoric dissolved organic matter (CDOM) in a given water, consistent with the rapid depletion of a photo-labile DOM fraction. Together, the results suggest that the extent of light absorption by CDOM, aromatic carbon content, and iron concentration control the magnitude and shape of $\varphi_{PM,\lambda}$, which in turn strongly influences rates of photomineralization and CO_2 production in inland surface waters. Experiments to quantify $\varphi_{PM,\lambda}$ should consider that greater cumulative light absorbed leads to underestimates of $\varphi_{PM,\lambda}$ and photomineralization rates.

Received 16th April 2025
Accepted 27th July 2025

DOI: 10.1039/d5em00293a

rsc.li/espi

Environmental significance

Photomineralization of dissolved organic matter (DOM) to carbon dioxide (CO_2) in inland waters is important in the arctic carbon cycle. Photomineralization depends strongly on the apparent quantum yield spectrum ($\varphi_{PM,\lambda}$), *i.e.*, the wavelength-dependent efficiency of DOM conversion to CO_2 by sunlight. Labor-intensive approaches to quantify $\varphi_{PM,\lambda}$ have resulted in few direct measurements of $\varphi_{PM,\lambda}$, thus limiting knowledge of its controls. To address this knowledge gap, an LED-based approach was used to directly quantify the wavelength-dependent magnitude of $\varphi_{PM,\lambda}$ in arctic streams and lakes where DOM composition and water chemistry has been well characterized. $\varphi_{PM,\lambda}$ is a function of sunlight exposure history, aromatic DOM, and dissolved iron. These findings may explain some differences in $\varphi_{PM,\lambda}$ between arctic, boreal, and temperate-zone freshwaters.

1 Introduction

Carbon dioxide (CO_2) emissions from inland surface waters to the atmosphere are nearly as large as the net carbon transfer from the atmosphere to the land surface during photosynthesis and respiration.[1–6] The export of dissolved organic matter (DOM) from land to inland surface waters contributes to this large flux because DOM is oxidized to CO_2 by microorganisms and sunlight in surface waters.[2,5,7] Sunlight degradation of DOM (photodegradation) can account for up to 95% of the DOM oxidized in inland surface waters.[7] Some of this DOM is completely oxidized to CO_2 (*i.e.*, photomineralization), which may contribute 10 to 30% of the total CO_2 emitted from inland surface waters to the atmosphere.[7–11]

Water column photomineralization rates are the product of two wavelength-dependent spectra. The first is the apparent quantum yield spectrum of DOM photomineralization ($\varphi_{PM,\lambda}$) as a function of wavelength from the ultraviolet (UV) to the visible, which is quantified as the moles of CO_2 produced per mole of photons absorbed by light-absorbing (chromophoric) DOM (CDOM). The second is the spectrum of the photon flux absorbed by CDOM over the depth of the water column. While the latter is well-characterized and depends strongly on the photon flux of sunlight reaching the water surface,[7] the apparent quantum yield spectrum $\varphi_{PM,\lambda}$ is poorly constrained because it has been difficult to measure.[12]

[a]*Department of Earth and Environmental Sciences, University of Michigan, Ann Arbor, MI, 48109, USA. E-mail: rmcory@umich.edu*

[b]*Department of Ecology and Evolutionary Biology, University of Michigan, Ann Arbor, MI, 48109, USA*

† Present address: Michigan Department of Environment, Great Lakes, and Energy, Lansing, MI 48909.

‡ Present address: Department of Ecology, Evolution, and Behavior, University of Minnesota, St. Paul, MN 55108.

Due to the difficulty of conventional methods for directly quantifying $\varphi_{PM,\lambda}$ of DOM as a function of wavelength (described in Ward *et al.*),[12] very few studies have quantified the magnitude and shape of the $\varphi_{PM,\lambda}$ spectrum. Those studies that directly quantified the shape of $\varphi_{PM,\lambda}$ found that it decreased exponentially with increasing wavelength from the UV to the visible portion of the solar spectrum.[13–15] Thus, most studies have estimated $\varphi_{PM,\lambda}$ using previously published exponential shapes of $\varphi_{PM,\lambda}$ that set the relative importance of UV and visible wavelengths.[7,16] However, calculations of photomineralization rates are quite sensitive to the exponential shape of the spectrum (Fig. 1),[17] and the shape of this spectrum is better characterized by a new light-emitting diode (LED) approach that has enabled rapid, direct quantification of the wavelength-dependence of photochemical reactions.[12,17] The magnitude and shape of $\varphi_{PM,\lambda}$ determined using this new approach varied more widely than shown in the few existing spectra[14,15] that have served as the basis for model fits used to estimate $\varphi_{PM,\lambda}$.[7,16,18] To better understand this variation, recent work has focused on determining the specific controls on $\varphi_{PM,\lambda}$.

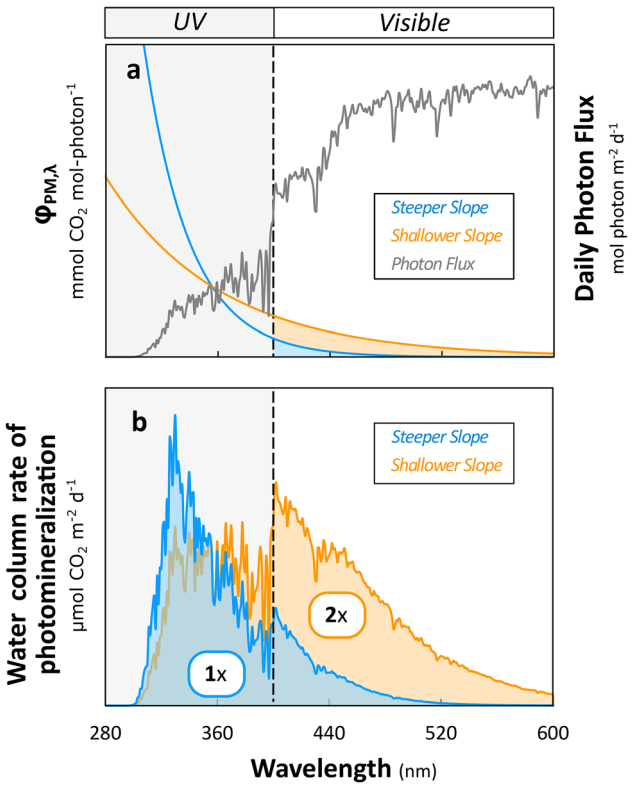

Fig. 1 Rates of DOM photomineralization in sunlit surface waters depend strongly on the wavelength-dependence of the AQY spectrum ($\varphi_{PM,\lambda}$). (a) Two hypothetical $\varphi_{PM,\lambda}$ spectra (primary *y*-axis) are superimposed on a clear-sky solar spectrum from the Alaskan Arctic (secondary *y*-axis). The integrated CO_2 yields (areas under the curves) for both $\varphi_{PM,\lambda}$ curves are equal, but the shallower slope leads to greater photomineralization yields than the steeper slope in the visible region, which contains over 90% of the daily photon flux. (b) Water column rates of photomineralization calculated from the product of each of the two $\varphi_{PM,\lambda}$ spectra and the same photon flux spectrum shown in (a). Integrated water column rates of photomineralization (areas under the curves) calculated using the shallower $\varphi_{PM,\lambda}$ slope are double (2×) those calculated using the steeper $\varphi_{PM,\lambda}$ slope (1×).

Using this new LED approach, Bowen *et al.*[17] found that dissolved iron concentrations explained the variability in the magnitude of $\varphi_{PM,\lambda}$ for DOM leached from arctic permafrost soils. In addition to iron, DOM chemical composition is expected to affect the lability of DOM to photomineralization among surface waters and over seasonal time scales.[19–23] However, there are conflicting results on the relationships between DOM composition and $\varphi_{PM,\lambda}$. For example, one study found that the magnitude of $\varphi_{PM,\lambda}$ in lakes ranging in latitude from boreal to tropical increased with increasing aromatic content of DOM,[9] while another found that $\varphi_{PM,\lambda}$ in temperate lakes decreased with increasing aromatic content.[24] Another study found no relationship between DOM composition and $\varphi_{PM,350}$ for more than 100 samples from arctic lakes and streams.[7] Thus, there is uncertainty about how the magnitude of $\varphi_{PM,\lambda}$ depends on spatial or seasonal changes in DOM composition.

The conflicting results in the literature on the dependence of $\varphi_{PM,\lambda}$ on the aromatic content of DOM may be due to differences in the amount of light absorbed by CDOM during experimental quantification of $\varphi_{PM,\lambda}$. CDOM concentration is a function of the aromatic content of DOM,[25] and thus CDOM and aromatic carbon content co-vary in space and time in inland waters.[26] $\varphi_{PM,\lambda}$ spectra are often measured from a suite of natural waters spanning different CDOM concentrations and different aromatic carbon contents. Most often, studies expose each water sample to the same duration and irradiance of light, resulting in all waters receiving the same total amount of incoming light (referred to here as the "light dose"). However, the amount of the light dose that is absorbed by CDOM in the water samples depends on the initial CDOM concentration. Waters high in initial CDOM, with higher aromatic carbon content, will absorb more of the experimental light dose than waters low in initial CDOM. Thus, studies have differed substantially in the cumulative light absorbed by CDOM during quantification of $\varphi_{PM,\lambda}$. The most photo-labile DOM should be mineralized first and by the lowest amounts of cumulative light absorbed by CDOM. Conversely, increasingly less photo-labile DOM is mineralized later and at higher amounts of cumulative light absorbed. Thus, studies that standardize the light doses or light exposure times used to quantify $\varphi_{PM,\lambda}$, rather than the cumulative light absorbed by CDOM, are likely comparing $\varphi_{PM,\lambda}$ of portions of the DOM pool that differ in their lability to photomineralization. If the most photo-labile DOM is aromatic in nature, only studies that standardize experiments to the cumulative light absorbed by CDOM, rather than the light dose or light exposure time, will be able to determine the dependence of $\varphi_{PM,\lambda}$ on aromatic carbon content or other DOM characteristics. Thus, a critical knowledge gap is quantifying how $\varphi_{PM,\lambda}$ depends on the cumulative light absorbed by CDOM.

Many studies have reported decreasing rates of DOM photodegradation with increasing irradiation time and with increasing light reaching surface waters,[27–31] and have often attributed these decreases to loss of photo-labile DOM. Photomineralization and related photodegradation reactions that are

initiated by the absorption of light by CDOM alter DOM composition,[13,28,32] removing or altering portions of the DOM pool that are most labile to oxidation by sunlight. As these highly photo-labile components of the DOM pool are depleted, the remaining DOM is less labile to photodegradation. Therefore, as the cumulative amount of light absorbed by CDOM increases, the magnitude of $\varphi_{PM,\lambda}$ may decrease. However, no studies have investigated the dependence of $\varphi_{PM,\lambda}$ on the cumulative amount of light absorbed by CDOM. Two studies have quantified apparent quantum yields for products of DOM photodegradation other than CO_2 as a function of the cumulative amount of light absorbed by CDOM.[13,33] In one of these studies, Andrews *et al.* showed that the apparent quantum yields for photochemical oxygen consumption by DOM decreased with increasing cumulative light absorbed by CDOM in a nearshore marine environment where there was high sunlight and the DOM photodegradation capacity was estimated to be greater than the amount of DOM available.[13] This scenario of decreasing apparent quantum yield with increasing cumulative light absorbed was termed "substrate limitation" of DOM photodegradation.[34] In natural waters, the cumulative light absorbed by a pool of DOM increases with increasing residence time in sunlit surface waters, referred to as the light exposure history of DOM.[7] It is not known how increasing sunlight exposure of DOM over its residence time in inland surface waters might affect substrate limitation and the magnitude of $\varphi_{PM,\lambda}$.

The wavelength-dependent shape of $\varphi_{PM,\lambda}$ may also depend on light exposure history if there are wavelength dependencies of the specific mechanisms for DOM photomineralization or if there are pools of DOM that are labile to wavelength-dependent mechanisms of photomineralization. For example, photodecarboxylation is thought to be one mechanism of DOM photomineralization,[17,35,36] which may be relatively more efficient in the UVA and visible region compared to other mechanisms for DOM photomineralization.[17] In contrast to photodecarboxylation, the oxidation of DOM by reactive oxygen species (ROS) might dominate CO_2 yields at UVB wavelengths because the yields of photochemically-produced ROS are highest in the UVB region.[13,37–39] A greater depletion of the photo-labile DOM at UVA and visible *versus* UVB wavelengths of light would cause $\varphi_{PM,\lambda}$ to decrease relatively more at UVA and visible than at UVB wavelengths, resulting in a more steeply decreasing shape of $\varphi_{PM,\lambda}$ as sunlight exposure increases (*e.g.*, Fig. 1a). Despite evidence that the wavelength-dependent shape of $\varphi_{PM,\lambda}$ may depend on light exposure history, prior studies demonstrating both diminishing rates and diminishing apparent quantum yields for DOM photodegradation over time during light exposure have used broadband light sources that lack information about yields at individual wavelengths.[27–31,33] Thus, quantification of the relative steepness of the exponentially-decreasing spectral shape of $\varphi_{PM,\lambda}$ may provide new evidence on the mechanisms controlling DOM photomineralization or on the DOM pool sizes labile to different mechanisms.

To address these knowledge gaps, we used an LED-based approach to directly quantify the wavelength-dependent magnitude of $\varphi_{PM,\lambda}$ for arctic lakes and streams ranging in DOM composition and water chemistry. Multiple $\varphi_{PM,\lambda}$ spectra were quantified for each water with a range of cumulative light exposure histories to determine how $\varphi_{PM,\lambda}$ varies both among surface waters with different water chemistry and over time during the residence time of DOM in sunlit waters.

2 Methods

2.1 Site description, water sampling, and water analysis

Water samples for chemistry analysis were collected from six surface waters near the Arctic Long-Term Ecological Research (LTER) site at Toolik Lake,[40] Alaska during the ice-free summer months (May–August) of 2010–2022, as described in detail in the SI. Surface water sites included streams (Imnavait Creek and the Kuparuk River) and lakes (Toolik Lake and three lakes on the coastal plain of the Alaskan North Slope; Table S1).

Water temperature, pH, and specific conductance were measured in the field.[20,41] All water samples were filtered, acidified to pH 2, and analyzed for water chemistry and DOM composition as described in the SI. Water chemistry parameters measured included dissolved organic carbon (DOC), total dissolved iron, CDOM, and the fluorescent fraction of DOM (FDOM). CDOM and FDOM data were used to calculate proxies for DOM source and composition, including the spectral slope ratio (S_R), specific UV absorbance at 254 nm ($SUVA_{254}$), fluorescence index (FI), and peak T/A ratio.

A subset of the water samples collected for chemistry analysis were used in LED light exposure experiments to quantify the photomineralization apparent quantum yield ($\varphi_{PM,\lambda}$). Immediately after surface water collection, waters were GF/F filtered and stored at 4 °C until further use in the LED light exposure experiments (as described in Section 2.2 below). Values of $\varphi_{PM,\lambda}$ were measured from water collected at each of the six surface water sites in June–July, 2021 and May–July, 2022 (Table S2). Water was sampled and analyzed for $\varphi_{PM,\lambda}$ on multiple dates during the summers of 2021 and 2022 from all sites except the coastal plain lakes LS 1-05, LS 1-27, and LS 1-28, which were each sampled only once on one date each summer (Table S2). Water at each site and date was exposed to three or four different LED wavelengths and up to six light doses at each wavelength, for a total of 147 $\varphi_{PM,\lambda}$ measurements from the LED light exposure experiments (Table S2). In addition to the LED measurements of $\varphi_{PM,\lambda}$, waters from Imnavait Creek, Kuparuk River and Toolik Lake were exposed to natural sunlight (Table S8) for quantification of $\varphi_{PM,\lambda}$ as described in Section 2.3 below.

2.2 Photomineralization apparent quantum yields (LED experiments)

GF/F-filtered waters collected in the summers of 2021–2022 were used in light exposure experiments to directly quantify the wavelength-dependent apparent quantum yield of photomineralization ($\varphi_{PM,\lambda}$) following Ward *et al.*[12] Briefly, each water was equilibrated to room temperature (~24 h) and filled with no headspace in gas-tight, flat-bottomed, pre-combusted 11-mL quartz vials (10 cm path length). For each water, quartz vials were exposed to custom-built high-powered (≥100 mW),

narrow-banded (±10 nm) LEDs maintained close to room temperature with heat sinks and cooling fans, at each of two UVB wavelengths (275 nm and 305 nm), one UVA wavelength (365 nm), and one visible wavelength (405 nm) alongside dark controls. While very little radiation at 275 nm reaches the earth's surface, no LEDs were available in the range of UVB wavelengths from 280 to 305 nm. Therefore, the 275 nm LED wavelength was used as an end-member for $\varphi_{PM,\lambda}$ spectra in this study and represents the highest-energy UVB photons reaching surface waters from sunlight (*e.g.*, the small portion of the solar spectrum from 280–305 nm that is rapidly attenuated by DOM in surface waters). During each light exposure experiment, duplicate samples in quartz vials were exposed to light at each wavelength to quantify CO_2 production and O_2 consumption. For all waters, CO_2 production, quantified as a significant difference in dissolved inorganic carbon (DIC) between light-exposed and dark control waters, was measured using an Apollo DIC analyzer.[7] A significant difference in light minus dark DIC was quantified as no overlap between the average ±1 standard error of the light and dark replicates ($n = 2$). For most waters in this study, CO_2 from photomineralization was detectable when the light minus dark difference in DIC was greater than ~0.5% of the dark (initial) DIC concentration. A few waters had detectable CO_2 from photomineralization when the light minus dark difference in DIC was less than ~0.5% of the dark DIC concentration. Dark (initial) DIC concentrations ranged from 26 ± 2.7 μM in Imnavait Creek to 1645 ± 2 μM in one of the coastal plain lakes. O_2 consumption, quantified similarly to CO_2 as the difference in dissolved O_2 between light-exposed and dark control waters, was measured using membrane inlet mass spectrometry (MIMS).[41] Dark minus light differences in dissolved O_2 are detectable when the difference is larger than ~1 μM.

At each LED wavelength, $\varphi_{PM,\lambda}$ was calculated as the amount of CO_2 produced by photomineralization divided by the light absorbed by CDOM in light-exposed waters using eqn (S1). The amount of light absorbed by CDOM (mol photon m^{-2} nm^{-1}) was quantified for each vial from the LED photon flux spectrum reaching sample waters and the geometric mean of the absorption coefficients of CDOM in dark control and light-exposed waters, using eqn (S2).[7] The photon flux spectrum was quantified from the irradiance spectrum from each LED source, which was measured by radiometry as previously described.[17] Prior work has cross-validated measurements of the photon flux by radiometry with chemical actinometry.[17] $\varphi_{PM,\lambda}$ is reported as the average ±1 standard error (SE) of experimental replicate vials ($n = 2$).

For all waters, one $\varphi_{PM,\lambda}$ spectrum was quantified using LED irradiances that were chosen so that similar amounts of light were absorbed by CDOM at each wavelength and among waters (0.5 mol photon m^{-2}). Because CDOM absorbance decreases with increasing wavelength and varies between waters, the doses of light that waters were exposed to were different for each site and LED wavelength. To quantify the effect of varying the amount of cumulative light absorbed by CDOM on the magnitude of $\varphi_{PM,\lambda}$, additional $\varphi_{PM,\lambda}$ spectra were quantified for a subset of the GF/F-filtered waters from each site. These waters were exposed to additional doses of LED light in time course experiments by varying the duration of LED light exposure, resulting in cumulative amounts of light absorbed by CDOM ranging from 0.05 mol photon m^{-2} to 2.85 mol photon m^{-2}.

For each water from LED light exposure experiments, the wavelength-dependent yields at the LED wavelengths tested were fit to a least-squares exponential model for $\varphi_{PM,\lambda}$ in the form of:

$$\varphi_{PM,\lambda} = c e^{-d\lambda} \quad (1)$$

where parameters c (mol CO_2 mol photon^{-1}) and d (nm^{-1}) are positive constants that quantify the intercept and slope (or relative steepness of exponential decay) of the $\varphi_{PM,\lambda}$ spectrum, respectively.[15,18] Linear and exponential models of the relationship between DOM composition or water chemistry and values of $\varphi_{PM,\lambda}$ at UV and visible LED wavelengths quantified using 0.5 mol photon m^{-2} light absorbed by CDOM were tested as described in the SI. The measures of DOM composition (S_R, $SUVA_{254}$, FI, and peak T/A ratio) that were investigated as predictors of $\varphi_{PM,\lambda}$ are ratios derived from optical measurements and, thus, are independent of the concentration of DOM in the samples.

2.3 Photomineralization apparent quantum yields (sunlight experiments)

A subset of the GF/F-filtered waters used in LED light exposure experiments were also exposed to natural (broadband) sunlight to calculate one additional $\varphi_{PM,\lambda}$ spectrum for each water using previously described methods.[7] This additional $\varphi_{PM,\lambda}$ spectrum allowed for comparison with prior work that has relied on assumptions about the shape of $\varphi_{PM,\lambda}$ to produced modeled spectra from broadband light exposure experiments.[7] Briefly, each of these water samples was equilibrated to room temperature (~24 h) and filled with no headspace in pre-combusted, gas-tight 12-mL borosilicate exetainers (1.5 cm path length; Labco, Inc). Waters were exposed to natural (broadband) sunlight for approximately 12 hours at the Toolik Field Station in the Alaskan Arctic during the summer months, alongside dark controls. At the end of the 12-hour sunlight exposure, CO_2 production by photomineralization and O_2 consumption were quantified in four light-exposed and four dark control replicates in borosilicate exetainers for each of the waters, as described in prior sections.

For the light exposure experiments using natural sunlight, $\varphi_{PM,\lambda}$ spectra were calculated for each water using an unconstrained nonlinear optimization function as described previously[7] and summarized in the SI.

2.4 Water column photomineralization rates

Water column photomineralization rates in each surface water were calculated to test how the directly-quantified shapes of $\varphi_{PM,\lambda}$ from LED experiments affected photomineralization rates, compared to modeled shapes of $\varphi_{PM,\lambda}$ estimated from broadband light exposures in prior work. Daily water column photomineralization rates were calculated according to eqn

(S5), described in the SI, as the product of the apparent quantum yield ($\varphi_{PM,\lambda}$), the daily photon flux absorbed by CDOM in the water column of the stream or lake ($Q_{a\lambda}$), and the ratio of $\frac{aCDOM_\lambda}{atot_\lambda}$. Three different $\varphi_{PM,\lambda}$, with different spectral slopes (parameter d in eqn (1)) that were either the minimum or maximum slopes directly quantified from LED light exposures or the slope estimated using an unconstrained nonlinear optimization function, as described in Section S1.4 and in prior work,[7] were used to calculate three different photomineralization rates for each water.

3 Results

The site averages of $\varphi_{PM,\lambda}$ for waters exposed to all doses of UVB LED light ranged from 1.7 ± 0.0 to 21.5 ± 1.7 mmol CO_2 mol photon^{-1} at 275 nm and from 0.4 ± 0.2 to 4.9 ± 0.8 mmol CO_2 mol photon^{-1} at 305 nm (mean ± SE; Table 1). For waters exposed to all doses of longer-wavelength UVA and visible LED light, the site averages of $\varphi_{PM,\lambda}$ ranged from −0.3 ± 0.5 to 9.4 mmol CO_2 mol photon^{-1} at 365 nm and from 0.0 ± 0.1 to 5.6 mmol CO_2 mol photon^{-1} at 405 nm (Table 1). The percent DOC photomineralized to CO_2 in all experiments ranged from 1 to 12% (average of 3 ± 0.4%).

3.1 CDOM light absorption and the apparent quantum yield

The doses of 275 nm light from LEDs in this study ranged from 0.04 to 2.8 mol photon m^{-2} (Table S2). The experimental light doses at 275 nm were nearly completely absorbed by CDOM in most sample waters, resulting in the absorption of 0.04 to 2.1 mol photon m^{-2} by CDOM (Table S2). Because CDOM absorbs exponentially less light with increasing wavelength, relatively higher light doses were necessary at 305, 365, and 405 nm to produce detectable amounts of CO_2 in each water, compared to the light doses needed to detect CO_2 production at 275 nm. Light doses at these longer wavelengths ranged from 0.05 to as high as 40 mol photon m^{-2} in some waters (Table S2). At these longer wavelengths, where CDOM absorption is low, the rate of light absorption by CDOM is insufficient to absorb all of the experimental light dose over the course of the experiment. For example, at 405 nm, CDOM absorbed 0.04 to 3.5 mol photon m^{-2} of the light doses ranging from 0.07 to 40 mol photon m^{-2} (Table S2).

The total amount of CO_2 produced by photomineralization at all wavelengths increased with increasing light dose for most waters (Fig. S1). To determine how the efficiency of this CO_2 production depended on the light exposure history of DOM, $\varphi_{PM,\lambda}$ was plotted as a function of the cumulative amount of the

Table 1 Average photomineralization apparent quantum yields ($\varphi_{PM,\lambda}$) of DOM in inland arctic surface waters collected in 2021 and 2022 and exposed to LED light[a]

		$\varphi_{PM,\lambda}$ (mmol CO_2 mol photon^{-1})				
		Target amount of cumulative light absorbed by CDOM (mol photon m^{-2})				
Site	Wavelength	0.05	0.5	1.2	2	2.85
Imnavait Creek	275	21.5 ± 1.7 (2)	8.0 ± 0.9 (6)	4.4 ± 0.1 (1)	3.7 ± 0.1 (1)	—
	305	—	4.9 ± 0.8 (4)	2.5 ± 0.1 (1)	2.6 ± 0.1 (1)	—
	365	9.4 (1)	1.8 ± 0.3 (6)	0.6 ± 0.1 (1)	0.8 ± 0.0 (1)	1.2 ± 0.0 (1)
	405	5.6 (1)	1.2 ± 0.1 (6)	0.5 ± 0.1 (1)	0.3 ± 0.1 (1)	0.7 ± 0.1 (1)
Kuparuk River	275	12.7 ± 1.5 (2)	3.9 ± 0.4 (8)	2.3 ± 0.1 (2)	1.7 ± 0.0 (1)	—
	305	—	2.4 ± 0.6 (4)	1.2 ± 0.2 (1)	1.0 ± 0.1 (1)	—
	365	6.1 (1)	1.1 ± 0.2 (7)	0.8 ± 0.1 (1)	0.4 ± 0.1 (2)	0.4 ± 0.0 (1)
	405	1.3 (1)	0.7 ± 0.2 (7)	0.4 ± 0.0 (1)	0.3 ± 0.1 (2)	0.3 ± 0.0 (1)
Toolik Lake	275	7.5 ± 1.0 (1)	2.7 ± 0.2 (4)	2.8 ± 0.1 (2)	2.3 ± 0.0 (1)	—
	305	—	1.0 ± 0.2 (3)	1.3 ± 0.1 (1)	1.0 ± 0.0 (1)	—
	365	—	0.3 ± 0.2 (4)	0.3 ± 0.1 (2)	0.3 ± 0.2 (1)	0.3 ± 0.0 (1)
	405	—	0.2 ± 0.1 (4)	0.3 ± 0.2 (2)	0.2 ± 0.1 (1)	0.2 ± 0.0 (1)
LS 1-05	275	19.1 ± 3.6 (1)	2.5 ± 1.0 (2)	—	2.2 ± 0.0 (1)	—
	305	—	1.8 ± 0.1 (1)	—	1.0 ± 0.2 (1)	—
	365	—	0.3 ± 0.3 (2)	—	0.2 ± 0.1 (1)	−0.2 ± 0.1 (1)
	405	—	0.0 ± 0.1 (2)	—	0.1 ± 0.0 (1)	0.2 ± 0.1 (1)
LS 1-27	275	11.2 ± 4.4 (1)	3.7 ± 0.1 (2)	—	—	—
	305	—	1.9 ± 0.0 (1)	—	—	—
	365	—	1.4 ± 0.0 (2)	—	—	0.1 ± 0.0 (1)
	405	—	0.6 ± 0.0 (2)	—	—	0.1 ± 0.1 (1)
LS 1-28	275	7.1 ± 1.9 (1)	3.3 ± 0.6 (2)	—	—	—
	305	—	0.4 ± 0.2 (1)	—	—	—
	365	—	−0.3 ± 0.5 (2)	—	—	0.2 ± 0.0 (1)
	405	—	0.0 ± 0.3 (2)	—	—	0.2 ± 0.0 (1)

[a] $\varphi_{PM,\lambda}$ values are reported as the average ±1 SE of $\varphi_{PM,\lambda}$ spectra for waters from the same site collected on different days (n indicated in parentheses). When there is only one water sample from a site that received a given light treatment, values are reported as the average ±1 SE of experimental replicates of the same water sample ($n = 2$) except in cases in which there was only one experimental replicate for which no SE is reported.

light dose that was absorbed by CDOM during time course experiments. Using the cumulative light absorbed by CDOM as a measure of light exposure history accounts for different rates of light absorption among waters over time due to different initial CDOM concentrations, different wavelengths of light treatment, and photobleaching of CDOM (see Section S2.1). We present two sets of comparisons. The first set (Fig. 2) compares $\varphi_{PM,\lambda}$ across all waters and wavelengths from light doses that resulted in detectable $\varphi_{PM,\lambda}$ during time course experiments, including results generated from the lowest amounts of cumulative light absorbed in which only 275 nm light resulted in a detectable $\varphi_{PM,\lambda}$. The second set (Fig. S2) compares the percent difference in $\varphi_{PM,\lambda}$ for each water between two different cumulative amounts of light absorbed (~0.5 *versus* 2.0 mol photon m^{-2} absorbed). The latter comparison was chosen because all waters and wavelengths produced detectable CO_2 at ~0.5 and 2.0 mol photon m^{-2} absorbed (Fig. S1). Both sets of comparisons show that $\varphi_{PM,\lambda}$ decreased significantly with increasing cumulative light absorbed by CDOM in most waters, independent of the wavelength of light (Fig. 2 and S2). For example, most waters show that $\varphi_{PM,\lambda}$ quantified at 2.0 mol photon m^{-2} absorbed by CDOM was at least 20% lower at all wavelengths than $\varphi_{PM,\lambda}$ quantified using 0.5 mol photon m^{-2} absorbed (Fig. S2). In this second comparison (Fig. S2), the exceptions to this pattern were Imnavait Creek water exposed to 305 nm and 365 nm light and Toolik Lake water exposed to 405 nm light. These latter light treatments resulted in no significant difference between $\varphi_{PM,\lambda}$ quantified using 0.5 *versus* 2.0 mol photon m^{-2} absorbed by CDOM. At 275 nm, for which a wider range of cumulative light absorbed (0.05 to 2.1 mol photon m^{-2}) could be tested compared to the range at longer wavelengths (Fig. 2), greater decreases in $\varphi_{PM,275}$ with increasing light absorbed were observed when the cumulative light absorbed remained low. For example, $\varphi_{PM,275}$ decreased by 57 to 92% with increasing cumulative light absorbed by CDOM from 0.05 to 0.5 mol photon m^{-2}, and decreased relatively less with increasing cumulative light absorbed from 0.5 to 2.0 mol photon m^{-2} (Fig. 2a).

3.2 Water chemistry and DOM composition

In addition to the amount of light absorbed by CDOM, both water chemistry and DOM composition also controlled the magnitude of $\varphi_{PM,\lambda}$. Imnavait Creek had the lowest pH and specific conductance, the highest DOC and CDOM (quantified as a_{305}), and the highest dissolved iron concentrations (Table S3). The other waters had a wider range of specific conductance and lower concentrations of DOC, CDOM, and dissolved iron compared to Imnavait Creek (Table S3). DOM in Imnavait Creek

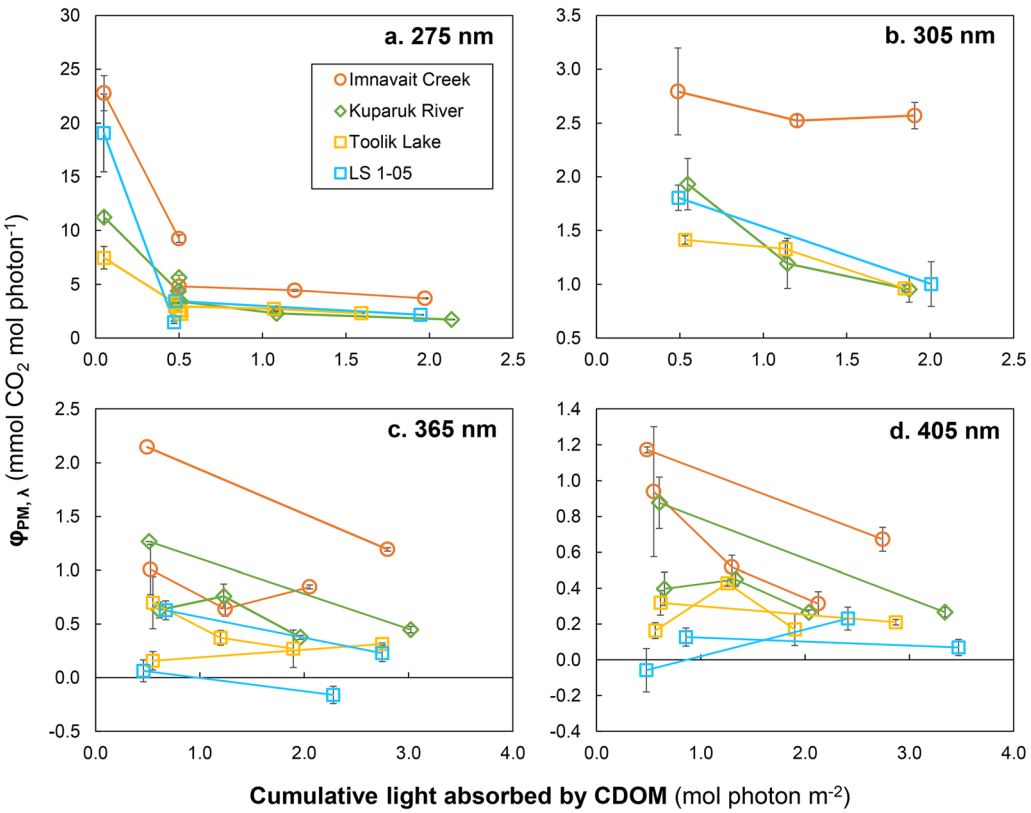

Fig. 2 The photomineralization apparent quantum yield ($\varphi_{PM,\lambda}$) decreases with increasing cumulative light absorbed by CDOM. DOM from Imnavait Creek (orange), the Kuparuk River (green), Toolik Lake (gold), and Lake LS 1-05 (blue) was exposed to LED light at (a) 275 nm, (b) 305 nm, (c) 365 nm, and (d) 405 nm. Multiple data series for a given site are for water samples collected on different dates. Each data series (data points connected by lines) indicates a single water sample exposed to multiple light doses. $\varphi_{PM,\lambda}$ values are shown as the average ±1 SE of experimental replicate vials ($n = 2$).

and the Kuparuk River had higher aromaticity (higher $SUVA_{254}$) and higher average molecular weight (lower S_R)[42] than DOM in the lake waters. DOM in stream waters had more terrestrially-derived DOM than DOM in lakes, based on the S_R values indicating higher average molecular weight and lower peak T/A ratio of stream *versus* lake DOM (see S1.1 and Table S3).

$\varphi_{PM,\lambda}$ quantified from 0.5 mol photon m^{-2} absorbed by CDOM was significantly, positively linearly correlated with total dissolved iron and with $SUVA_{254}$ ($p < 0.01$) (Fig. 3a and b) and significantly, negatively linearly correlated with S_R and peak T/A ($p < 0.01$; Fig. 3c and d) at both UV and visible wavelengths in the stream and lake waters studied. Exponential relationships between $\varphi_{PM,\lambda}$ and DOM composition and total dissolved iron were similarly or less significant than linear relationships (Fig. S3 and Table S4). Linear and exponential fitting parameters for $\varphi_{PM,\lambda}$ at all wavelengths as a function of DOM composition and water chemistry are provided in the SI.

3.3 Shape of the apparent quantum yield spectrum

The $\varphi_{PM,\lambda}$ spectra directly quantified from LED light exposures in which approximately 0.5 mol photon m^{-2} was absorbed by CDOM at all wavelengths had shapes that decreased approximately exponentially with increasing wavelength (Fig. S4), consistent with prior work.[12–15] The steepness of the exponential fits for the shape of $\varphi_{PM,\lambda}$ spectra is determined by the spectral slope d in eqn (1). The spectral slopes of $\varphi_{PM,\lambda}$ spectra across all sites and light doses in this study ranged from 0.010 to 0.028 nm^{-1}, with an average of 0.017 ± 0.001 nm^{-1} ($n = 34$; Table S6). In contrast, the average spectral slope of $\varphi_{PM,\lambda}$ spectra for the same sites used in this study was previously found to be 0.022 ± 0.000 nm^{-1} ($n = 42$) when $\varphi_{PM,\lambda}$ spectra were fit using an unconstrained nonlinear optimization function with a predetermined initial estimate of 0.03 nm^{-1} for the spectral slope.[7] Thus, spectral slopes of $\varphi_{PM,\lambda}$ spectra directly quantified from LED light exposures were on average shallower than slopes of modeled $\varphi_{PM,\lambda}$ spectra for broadband light exposures of waters from the same lakes and streams tested in prior work.[7]

4 Discussion

Overall, the differences in DOM optical properties between stream and lake waters are consistent with prior work in these same waters showing a stronger signature of terrestrially-derived DOM in stream *versus* lake waters, such as higher aromaticity of DOM in streams *versus* lakes using ^{13}C-NMR.[26,43] Values of $\varphi_{PM,\lambda}$ are also consistent with prior work. For example, the values of $\varphi_{PM,305}$ in this study span the same orders of magnitude as previously reported $\varphi_{PM,305}$ of arctic freshwaters (<0.1 to 14 mmol CO_2 mol photon^{-1} at 305 nm)[7] and $\varphi_{PM,309}$ of arctic permafrost soil leachates (0.4 to 2.3 mmol CO_2 mol photon^{-1}).[17] Additionally, values of $\varphi_{PM,365}$ encompass the range of $\varphi_{PM,365}$ previously reported for DOM isolates (0.09 to 0.11 mmol CO_2 mol photon^{-1}) and for DOM in boreal, temperate, and tropical lakes (0.09 to 1.3 mmol CO_2 mol photon^{-1}).[9,24] By directly quantifying the wavelength-dependent magnitude of $\varphi_{PM,\lambda}$ as a function of cumulative light absorbed

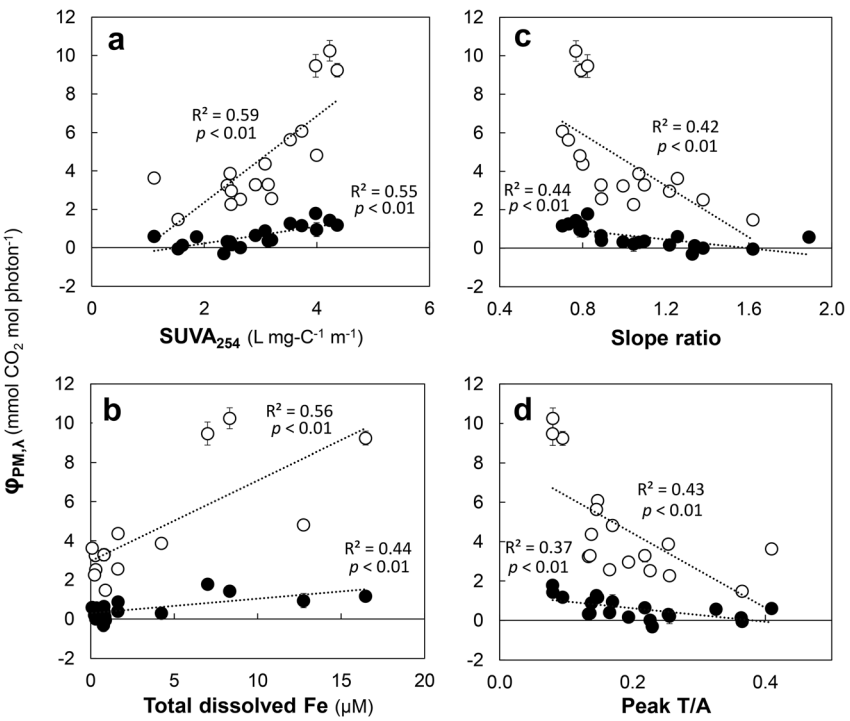

Fig. 3 $\varphi_{PM,\lambda}$ at 275 nm (open circles) and 405 nm (filled circles) was correlated with water chemistry and DOM composition. $\varphi_{PM,\lambda}$ increased with increasing (a) $SUVA_{254}$ and (b) total dissolved iron (Fe) concentrations and with decreasing (c) slope ratio and (d) peak T/A. Data were fit using least-squares regressions. $\varphi_{PM,\lambda}$ values are shown as the average ±1 SE of experimental replicates ($n = 2$). Where y-axis error bars are not visible, they are smaller than the data points.

by CDOM for the first time, this study demonstrates that light exposure history and DOM composition affect the magnitude and shape of $\varphi_{PM,\lambda}$.

4.1 The effects of CDOM light absorption on apparent quantum yields

A pattern of decreasing rates of DOM photodegradation with increasing light exposure observed in many prior studies has been interpreted as the removal of the most highly photo-labile components of the DOM pool at the lowest amounts of light exposure, leaving behind less photo-labile components.[27–31] Apparent quantum yields for many DOM photodegradation processes have long been assumed to decrease with increasing light exposure history in response to this decreasing photolability of DOM. However, apparent quantum yields for DOM photodegradation have only been quantified as a function of light exposure for two waters in prior work.[13,33] Here, we directly quantified the wavelength-dependent effects of increasing cumulative light exposure history on $\varphi_{PM,\lambda}$ for water samples from six different inland arctic surface waters. We show that $\varphi_{PM,\lambda}$ is strongly dependent on the cumulative amount of light absorbed by CDOM at all wavelengths, decreasing by up to 92% with increasing light absorbed (Fig. 2).

The extent to which $\varphi_{PM,\lambda}$ decreased with increasing cumulative light absorbed by CDOM is similar to a prior study of photo-oxidation of DOM. In the prior study, the apparent quantum yield for photo-oxidation of DOM, which is positively correlated with photomineralization during photodegradation,[7] decreased by 70% with an increase in cumulative UVB light absorbed from approximately 0.01 to 0.4 mol photon m^{-2} for terrestrially-derived DOM in nearshore marine water, determined using an experimental pathlength of light similar to that used in this study.[13] This decrease in the yield for photo-oxidation with increasing light exposure falls within the range of 57 to 92% decrease in $\varphi_{PM,275}$ for an increase in cumulative 275 nm light absorbed by CDOM from 0.05 to 0.5 mol photon m^{-2} for Imnavait Creek, the Kuparuk River, and Toolik Lake in this study (Fig. 2a).

4.2 The effects of dissolved iron and DOM composition on apparent quantum yields

The significant positive correlation between $\varphi_{PM,\lambda}$ and iron (Fig. 3b) supports prior work demonstrating the role of iron in increasing the yield of CO_2 from DOM photomineralization.[17,44] Iron is thought to catalyze the oxidation of carboxylic acids within DOM to CO_2 (*i.e.*, photo-decarboxylation).[17,36,45,46] Photo-decarboxylation is a ligand–metal interaction whereby Fe(III) complexed by carboxylic acids within DOM acts as a catalyst for the oxidation of the carboxyl acids to CO_2.[17,46] Here, we provide evidence that some of these carboxylic acids are aromatic.

$SUVA_{254}$ is a proxy for the aromatic carbon content of DOM.[25] The significant, positive correlation between $\varphi_{PM,\lambda}$ and $SUVA_{254}$ (Fig. 3a), suggests that the DOM most labile to photomineralization has high aromatic content. The decrease in $\varphi_{PM,\lambda}$ with increasing slope ratio (Fig. 3c), a proxy for the average molecular weight of DOM,[42] shows that the DOM most labile to photomineralization has relatively high molecular weight. These relationships between $\varphi_{PM,\lambda}$ and water chemistry suggest that terrestrially-derived DOM characterized by high aromaticity and high molecular weight draining into inland arctic surface waters makes up the fraction of the DOM pool that is most highly labile to photomineralization. High lability of aromatic DOM to photomineralization is consistent with many studies showing loss of aromatic DOM concurrent with DOM conversion to CO_2 during light exposure.[32,47–49] Loss of aromatic DOM has also been observed concurrently with a high loss of carboxyl carbon during sunlight exposure of DOM draining from permafrost soils.[32] Thus, results from this study support prior work showing that the carboxylic acids most labile to photomineralization to CO_2 are associated with aromatic fractions of DOM.

The strong dependence of $\varphi_{PM,\lambda}$ on dissolved iron and the chemical composition of DOM predicts that $\varphi_{PM,\lambda}$ at all wavelengths will vary substantially as a result of spatial and temporal variation in water chemistry and DOM composition, both in surface waters of the Arctic and surface waters at other latitudes spanning similar ranges of dissolved iron and DOM as in this study. Understanding how $\varphi_{PM,\lambda}$ depends on DOM composition is important given that the average composition of DOM exported to inland surface waters as the Arctic warms will change as an increasing proportion of that DOM comes from thawing permafrost soils. DOM draining from permafrost soil layers typically has lower aromatic content ($SUVA_{254}$ of 1.7 ± 0.1 L mg C^{-1} L^{-1})[17,50,51] than DOM draining from the thawed, surface active layer ($SUVA_{254}$ of 2.7 ± 0.4 L mg C^{-1} L^{-1}).[50,51] However, DOM draining from permafrost soils is also associated with relatively high dissolved iron.[17,52,53] Based on the results of this study, $\varphi_{PM,\lambda}$ is predicted to decrease with decreasing aromaticity of DOM but increase with increasing dissolved iron. The net effect of shifting DOM sources on the magnitude of $\varphi_{PM,\lambda}$ might depend on the relative importance of aromaticity *versus* dissolved iron concentrations.

4.3 Standardizing the light absorbed in photochemical experiments

This study is the first to show that $\varphi_{PM,\lambda}$ is positively correlated with the aromatic content of DOM when the amount of light absorbed by CDOM is standardized across waters and light treatments (Fig. 3). It is expected that $\varphi_{PM,\lambda}$ should be positively correlated with aromatic carbon content of DOM, given that many studies show loss of aromatic DOM during light exposure.[32,47–49] However, most prior work found no correlation between $\varphi_{PM,\lambda}$ and the initial aromatic content of DOM,[7] or showed that $\varphi_{PM,\lambda}$ is negatively correlated with the initial aromatic content.[24] In the one prior study that reported a positive correlation between $\varphi_{PM,\lambda}$ and the aromatic content, the magnitude of $\varphi_{PM,\lambda}$ spanned a lower range (0.4 to 4.4 mmol CO_2 mol photon^{-1} at 275 nm) compared to that in the present study (1.5 to 10.2 mmol CO_2 mol photon^{-1} at 275 nm), over a similar range of aromatic content.[9] Differences between the relationships in this study and those in prior work are likely due to the lack of standardization of the amounts of light absorbed by CDOM.

When studies reported no relationship or a negative correlation between $\varphi_{PM,\lambda}$ and aromatic content, $\varphi_{PM,\lambda}$ was measured

from experiments where either the duration of light exposure or the total light dose was held constant for waters varying in CDOM concentration.[7,9,24] Because waters high in CDOM concentration both absorb light at a greater rate and are often high in their aromatic content,[34,54] waters containing highly aromatic DOM will absorb substantially more of a given light dose than will waters containing less aromatic DOM. Because the magnitude of $\varphi_{PM,\lambda}$ depends strongly on the cumulative amount of light absorbed by CDOM (Fig. 2), experiments quantifying $\varphi_{PM,\lambda}$ from a large amount of light absorbed in a high CDOM, high aromatic DOM water may miss the higher $\varphi_{PM,\lambda}$ corresponding to the most photo-labile DOM at the lowest amounts of light absorbed. Differences in the amounts of light absorbed between waters in a given study likely completely or partially outweighed the effect of aromatic content on $\varphi_{PM,\lambda}$.[7,9,24] Thus, the effects of DOM composition on $\varphi_{PM,\lambda}$ cannot be reliably distinguished from the effects of light exposure history in prior work in which light absorbed by CDOM was not standardized.

Nonetheless, the effects of DOM composition and light absorption on $\varphi_{PM,\lambda}$ may be evident over a large enough range of both these controls in the literature, compared to any individual study (Fig. 4 and Table S5). On average, $\varphi_{PM,350}$ values reported for inland arctic and boreal surface waters are higher than $\varphi_{PM,350}$ values reported for inland temperate and tropical surface waters (Fig. 4). The majority of the variation in the regional average $\varphi_{PM,350}$ can be explained by the composition of DOM. Latitudes in which waters have higher average aromatic content have higher $\varphi_{PM,350}$ values (Fig. 4b), consistent with the positive correlation between $SUVA_{254}$ and $\varphi_{PM,\lambda}$ at all wavelengths in this study (Fig. 3a and S3). However, some differences in $\varphi_{PM,350}$ among latitudes may not be explained by DOM composition alone. For example, arctic surface waters have a significantly higher average $\varphi_{PM,350}$ compared to temperate and tropical surface waters, despite having a similar average $SUVA_{254}$ to these waters. The average $\varphi_{PM,350}$ for arctic surface waters might be higher than predicted based on $SUVA_{254}$ because experiments to quantify $\varphi_{PM,350}$ in arctic waters used the lowest amounts of light absorbed by CDOM (1.1 ± 0.1 mol photon m^{-2}), which are expected to lead to relatively higher values for $\varphi_{PM,350}$ compared to experiments done with tropical and temperate waters that used greater amounts of light absorbed by CDOM (6.6 ± 1.0 and 11.3 ± 3.7 mol photon m^{-2}, respectively; Fig. 4a). Thus, both differences in DOM composition and the amount of light absorbed by CDOM likely contribute to variation in the magnitude of $\varphi_{PM,\lambda}$ in prior work.

4.4 Controls on the shape of the apparent quantum yield spectrum

Water column photomineralization rates depend strongly on the spectral slope of $\varphi_{PM,\lambda}$.[17] Thus, it is important to understand how the shapes of $\varphi_{PM,\lambda}$ generated for the same water using different methods may affect estimates of water column photomineralization rates. For example, water column photomineralization rates calculated for the same sunny summer-solstice day (21 June 2018) in Imnavait Creek, the Kuparuk River, and Toolik Lake with a $\varphi_{PM,\lambda}$ fit to the modeled spectral slope assumed in Cory *et al.*[7] were 6.6, 3.7, and 4.1 mmol CO_2 m^{-2} d^{-1}, respectively (Tables S7 and S8). Water column photomineralization rates calculated assuming that $\varphi_{PM,\lambda}$ had the steepest and shallowest spectral slopes measured directly in this study were 20 to 40% slower for the steepest slope and 20 to 45% faster for the shallowest slope, compared to water column rates calculated with spectral slopes modeled using assumptions from prior work (Table S7 and Fig. S5).[7]

Differences in total water column photomineralization rates calculated using different spectral slopes of $\varphi_{PM,\lambda}$ were primarily due to differences in rates at visible wavelengths. The shallower the $\varphi_{PM,\lambda}$ spectral slope, the relatively higher the yield at visible wavelengths compared to the yield at UV wavelengths (Fig. 1). For example, photomineralization at visible wavelengths accounted for 57 to 68% of total photomineralization

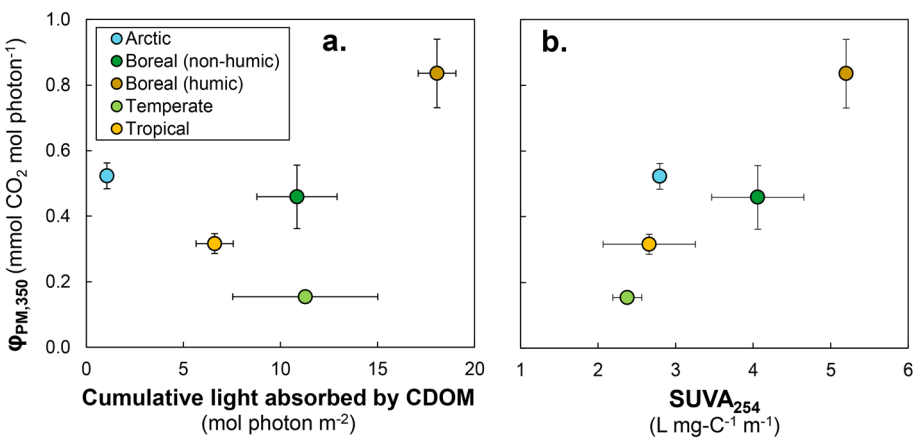

Fig. 4 The average photomineralization apparent quantum yield at 350 nm ($\varphi_{PM,350}$) reported in prior work for inland surface waters at different latitudes as a function of (a) light absorbed by CDOM and (b) $SUVA_{254}$. $\varphi_{PM,350}$ values, light absorbed by CDOM, and $SUVA_{254}$ are shown as the average ±1 SE of all $\varphi_{PM,350}$ values reported at each latitude (*n* provided in Table S5). Average $\varphi_{PM,350}$ values include apparent quantum yields reported at both 350 nm (Cory *et al.*, 2014; Koehler *et al.*, 2016; and Groeneveld *et al.*, 2016) and at 365 nm (Milstead *et al.*, 2023).

rates calculated using the shallower spectral slope, but only 29 to 46% of total photomineralization rates calculated using the steeper spectral slope (Table S7). Although the absorbance of light by CDOM is much higher in the UV than in the visible region, more total visible light reaches the water surface, and thus more visible light is absorbed by CDOM in the water column, compared to the amount of UV light absorbed.[55] Therefore, relatively higher or lower yields of CO_2 at visible wavelengths resulted in substantially faster or slower photomineralization rates, respectively (*e.g.*, Fig. S5). Because the directly-quantified $\varphi_{PM,\lambda}$ slopes in this study are on average shallower (with higher yields at visible wavelengths) than the modeled slopes assumed in Cory *et al.*[7] (and other studies), water column rates of photomineralization in these arctic surface waters may be greater than previously reported.

The extent of light exposure of DOM may be a control on the spectral slope of $\varphi_{PM,\lambda}$. The spectral slope of $\varphi_{PM,\lambda}$ increased with increasing cumulative light absorbed by CDOM in Imnavait Creek (Fig. S6a), while there was no relationship between the spectral slope of $\varphi_{PM,\lambda}$ and cumulative light absorbed in the Kuparuk River or Toolik Lake (Fig. S6b). Steeper spectral slopes with increasing cumulative light absorbed in Imnavait Creek indicate that $\varphi_{PM,\lambda}$ decreased relatively more at visible wavelengths than at UV wavelengths during light exposure. Thus, the portion of DOM in Imnavait Creek that is most labile to photomineralization is likely more rapidly depleted at visible wavelengths relative to UV wavelengths. Because this dependence of the slope of $\varphi_{PM,\lambda}$ on cumulative light absorbed was not observed in waters from other sites, the fraction of DOM that was highly labile to photomineralization at visible wavelengths in Imnavait Creek is inferred to compose less of the photo-labile DOM in the Kuparuk River and Toolik Lake.

DOM in Imnavait Creek might be relatively more labile to photomineralization at visible wavelengths because this site typically has the highest concentrations of dissolved iron of the waters sampled (Table S3). When complexed with carboxyl carbon in DOM, dissolved iron may catalyze the photomineralization of this DOM through photodecarboxylation.[17,36,45,46] Compared to other mechanisms of photomineralization (*e.g.*, oxidation of DOM by hydroxyl radical),[20] photodecarboxylation might have higher yields in the visible relative to the UV region. For example, DOM inferred to be complexed with dissolved iron has been shown to increase absorption of visible wavelengths of light compared to absorption in the absence of iron.[56] The latter evidence, combined with studies of model complexes of iron and organic ligands,[46] suggests that iron might catalyze more photodecarboxylation of DOM at visible than at UV wavelengths.[17,45] Consistent with this expectation, Bowen *et al.*[17] found that the molar ratio of photochemical CO_2 production to O_2 consumption, a proxy for the extent of decarboxylation, is greater at visible than at UV wavelengths. Thus, decarboxylation of iron-DOM complexes and the resulting depletion of this highly photo-labile fraction of DOM might explain the relatively greater decrease in $\varphi_{PM,\lambda}$ with increasing cumulative light absorbed at visible *versus* UV wavelengths in Imnavait Creek.

4.5 Substrate limitation of photomineralization rates

Water column photomineralization rates in streams and lakes are determined by (1) the amount of downwelling sunlight reaching the water surface, (2) the amount of CDOM available to absorb that downwelling sunlight, and (3) the lability of DOM to photomineralization, quantified as $\varphi_{PM,\lambda}$. The first control relates to the supply of light, while the latter two controls relate to the supply (quantity and quality) of the DOM substrate. Thus, either the supply of light, the supply of substrate, or both may limit photomineralization rates.[34] The results of this study provide new information about substrate limitation of photomineralization in inland surface waters.

Surface waters are substrate-limited if photomineralization rates increase with increases in the quantity or quality of the DOM substrate. Prior work has largely focused on the quantity of CDOM available to absorb sunlight reaching the water surface as a cause of substrate limitation.[34] However, photomineralization rates also depend on the quality of the substrate in surface waters. Our results show that $\varphi_{PM,\lambda}$ decreases with increasing cumulative light absorbed by CDOM, which is inferred to reflect the depletion of the most photo-labile fractions of DOM. Even when there is sufficient CDOM, photomineralization rates can respond to depletion of the photo-labile fraction with increasing light exposure history. In practice, substrate limitation by CDOM concentrations and by DOM photo-lability ($\varphi_{PM,\lambda}$) are expected to be correlated because progressive sunlight exposure of DOM results in both photobleaching (loss) of CDOM and depletion of the most photo-labile fraction of the DOM pool.[7,13] Predicting how strongly photomineralization rates are substrate-limited by DOM photo-lability requires knowing how much the magnitude of $\varphi_{PM,\lambda}$ changes over light-exposure time in surface waters.

At all sites, the maximum value of $\varphi_{PM,\lambda}$ for each water (*i.e.*, the value of $\varphi_{PM,\lambda}$ quantified using the smallest amount of light absorbed by CDOM that yielded detectable product at a given wavelength) is the best estimate of the instantaneous lability of DOM to photomineralization. This is because $\varphi_{PM,\lambda}$ values quantified using larger amounts of light absorbed by CDOM reflect depletion of photo-labile DOM in the closed system of light exposure experiments, compared to a natural system with turnover of photo-labile DOM. Because some depletion of the most photo-labile DOM likely occurred before even the smallest amount of light tested in LED experiments in this study was absorbed by CDOM, this maximum $\varphi_{PM,\lambda}$ is still an underestimate. At present, therefore, all estimates of $\varphi_{PM,\lambda}$ – including those reported in this study – are biased low because a detectable product must be formed in order to experimentally quantify $\varphi_{PM,\lambda}$. Furthermore, previous studies have typically quantified $\varphi_{PM,\lambda}$ using amounts of light absorbed that are greater than even the largest amount of light absorbed in this study (Fig. 4a). Because $\varphi_{PM,\lambda}$ decreased from 8 to 92% with increasing cumulative light absorbed, and $\varphi_{PM,\lambda}$ in over half of the waters tested decreased by at least 40%, $\varphi_{PM,\lambda}$ in prior work is likely underestimated by at least this much.

4.6 The effects of DOM turnover time in natural waters

While light exposure experiments can yield best estimates of $\varphi_{PM,\lambda}$ at the time of water sample collection, scaling-up photomineralization rates to longer time scales requires consideration of how light exposure history affects the loss of photo-labile substrates and thus the value of $\varphi_{PM,\lambda}$. Unlike in our experiments, where photo-labile DOM depleted during light exposure was not replenished, inland surface waters receive fresh, potentially photo-labile DOM from soil waters, sediments, and autochthonous production.[3,34,57,58] Thus, at longer time scales, the turnover rate of photo-labile DOM is a net balance between input and removal rates. If the pool of photo-labile DOM in the water column is removed by sunlight exposure (or other processes including microbial respiration, lateral transport, or burial)[3,7,26] faster than it is replenished over the residence time of DOM in the water column, then we expect the pool of photo-labile DOM to decrease, substrate limitation to increase, and $\varphi_{PM,\lambda}$ to decrease over time.

The turnover of photo-labile DOM in natural systems is difficult to measure directly, but it can be inferred from changes over time in the magnitude of $\varphi_{PM,\lambda}$. The magnitude of $\varphi_{PM,\lambda}$ was shown in this study to be positively, linearly correlated with dissolved iron concentration and with $SUVA_{254}$, a proxy for the aromatic content of the DOM (Fig. 3). Because iron concentrations and $SUVA_{254}$ are each much easier to quantify than are $\varphi_{PM,\lambda}$ spectra, they can predict seasonal variation in the magnitude of $\varphi_{PM,\lambda}$. In turn, understanding seasonal changes in $\varphi_{PM,\lambda}$ provides information about substrate limitation and the turnover of photo-labile DOM in surface waters.

When the relationship between $\varphi_{PM,\lambda}$ and $SUVA_{254}$ is extrapolated to the range of $SUVA_{254}$ observed in these waters over the summer season (Table S9), patterns of substrate limitation by $\varphi_{PM,\lambda}$ are observed in the streams and lakes (Fig. 5). For example, after increasing sharply during spring thaw, $\varphi_{PM,275}$ predicted from $SUVA_{254}$ in Imnavait Creek remains relatively constant around an average of 7.6 ± 0.1 mmol CO_2 mol photon^{-1} through July (mean ± SE of all $\varphi_{PM,275}$ predicted from $SUVA_{254}$ measurements from Imnavait Creek between May 20 and July 31 in 2016; Fig. 5). Relatively constant $\varphi_{PM,275}$ over time, as is the case for most of July, indicates that substrate limitation changes little due to a net balance of photo-labile DOM removal and replenishment. The high $\varphi_{PM,275}$ predicted for Imnavait Creek from spring runoff in late May through July is consistent with knowledge of hydrologic controls on export of photo-labile DOM to Imnavait Creek. For example, during the wetter hydrologic states of spring runoff through mid-summer characterized by high lateral flows, high in-stream flows, and short in-stream residence times, DOM in Imnavait Creek is primarily composed of groundwater DOM.[57] Given that groundwater DOM exported to streams *via* lateral inflow has no light-exposure history, this DOM is expected to have the highest abundance of photo-labile DOM, and thus highest $\varphi_{PM,275}$ relative to larger streams or lakes, as observed in this study and prior work in these waters.[7] During August, however, a slight decrease in $\varphi_{PM,275}$ to a monthly average of 6.8 ± 0.1 mmol CO_2 mol photon^{-1} indicates that Imnavait Creek is receiving a smaller influx of photo-labile DOM, leading to lower photomineralization rates (Fig. 5). Imnavait Creek in August is characterized by low in-stream flows and longer water residence times when photomineralization of the groundwater DOC may deplete the most photo-labile DOC faster than it is replenished.

In the Kuparuk River, seasonal values of $\varphi_{PM,275}$ predicted from $SUVA_{254}$ are more variable (from 3.1 to 5.7 mmol CO_2 mol photon^{-1}, Fig. 5) than the values of $\varphi_{PM,275}$ predicted in Imnavait Creek. Periods of sustained decreases in $\varphi_{PM,275}$ during June and late July into August indicate a lower replenishment rate of the photo-labile DOM that is removed in the river. The same hydrologic processes resulting in the dominance of groundwater DOM in Imnavait Creek operate in the Kuparuk River, a higher order stream that includes Imnavait Creek and its watershed.[57] However, DOM in the larger Kuparuk River has spent more time in sunlit surface water relative to the

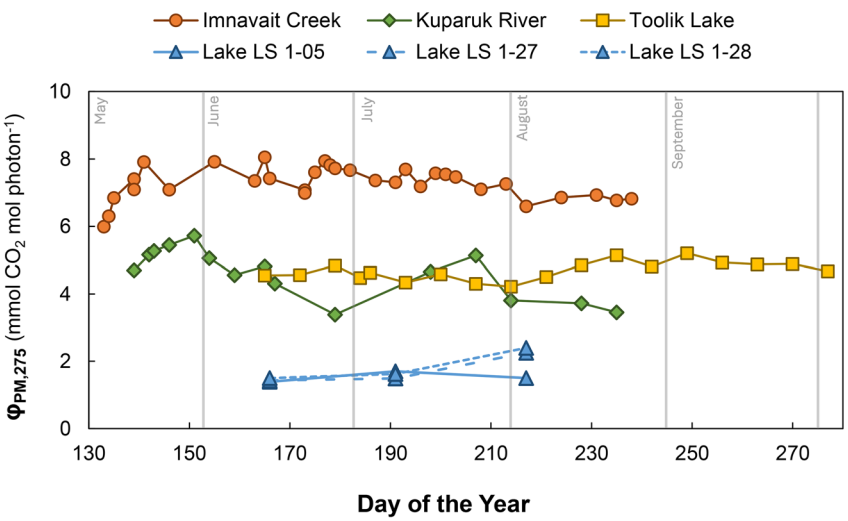

Fig. 5 $\varphi_{PM,275}$ values predicted from $SUVA_{254}$ of DOM in waters collected during the ice-free summer months from Imnavait Creek in 2016, the Kuparuk River in 2012, Toolik Lake in 2019, and the three coastal plain lakes LS 1-05, LS 1-27, and LS 1-28 in 2014.

DOM in the headwater Imnavait Creek. Thus, DOM in the Kuparuk River has a greater light-exposure history than in Imnavait Creek, resulting in removal of the most photo-labile DOM faster than it is replenished, as indicated by the lower $\varphi_{PM,275}$ (Fig. 5). Precipitation events like summer storms replenish the groundwater DOM in the Kuparuk River,[57] thus increasing the $SUVA_{254}$ and the predicted $\varphi_{PM,275}$ in the river.

In the lakes, values of $\varphi_{PM,275}$ predicted from $SUVA_{254}$ were relatively constant over the summer in both Toolik Lake (4.5 ± 0.1 mmol CO_2 mol photon^{-1}) and the coastal plain lakes (1.2 ± 0.1 mmol CO_2 mol photon^{-1} across all three lakes; Fig. 5). This result indicates that the turnover (net of the supply and loss rates) of the photo-labile DOM in these lakes is relatively constant over time. Seasonal values of $\varphi_{PM,\lambda}$ at the longer UV and visible wavelengths are predicted to show the same patterns of substrate limitation as observed at 275 nm over time because $\varphi_{PM,\lambda}$ at all wavelengths are strongly correlated with each other (Fig. S7).

5 Conclusions

The apparent quantum yield of photomineralization decreases with increasing cumulative light absorbed by CDOM, a proxy for the light exposure history of DOM. The decrease in $\varphi_{PM,\lambda}$ with increasing cumulative light absorbed by CDOM ranged from 8 to 92%, and was highest at the lowest amounts of light absorbed by CDOM. For $\varphi_{PM,\lambda}$ measured using the same amount of light absorbed by CDOM across all waters in this study, $\varphi_{PM,\lambda}$ was significantly, positively correlated with dissolved iron and $SUVA_{254}$ (a proxy for aromatic carbon content). The slope of $\varphi_{PM,\lambda}$ directly measured in this study was shallower than the slopes assumed from a modeled $\varphi_{PM,\lambda}$ spectrum in prior studies of the same waters, indicating greater photomineralization at longer, visible wavelengths.

There are several implications of the finding that $\varphi_{PM,\lambda}$ is strongly related to the amounts of light absorbed by CDOM and the requirement of a minimum amount of light necessary to achieve a detectable product. First, the effects of DOM composition on $\varphi_{PM,\lambda}$ may be clearest when measurements of $\varphi_{PM,\lambda}$ are made by standardizing the amount of light absorbed by CDOM across all waters. Furthermore, results from this study suggest substantial uncertainty in the composition of DOM most labile to photomineralization. In this study, which uses lower amounts of light absorption to quantify $\varphi_{PM,\lambda}$ compared to prior work, the percent DOC photomineralized to CO_2 averaged only $3 \pm 0.4\%$. In contrast, studies that examine the effect of photodegradation on DOM to infer fractions labile to photomineralization often conduct experiments with much greater loss of DOC by photomineralization to ensure detectable differences in DOM composition (17 to 46%).[36,49,59] Thus, at present it is not possible to identify the composition of the most photolabile DOM that is photomineralized at low amounts of light absorption by CDOM.

Second, previously reported values of $\varphi_{PM,\lambda}$ in inland waters[7–11] may be substantially underestimated. This is because $\varphi_{PM,\lambda}$ values quantified using larger amounts of light absorbed by CDOM reflect depletion of photo-labile DOM in the closed system of light exposure experiments that does not occur to the same degree in a natural, open water column. For example, given that $\varphi_{PM,\lambda}$ decreased from 8 to 92% (mean = 47%) across all waters, wavelengths, and ranges of light absorbed in our study (Fig. 2 and S2), and that photomineralization rates depend linearly on the magnitude of $\varphi_{PM,\lambda}$ in eqn (S5), it follows that photomineralization rates are underestimated by ~47%. The magnitude of underestimation of photomineralization rates may be conservative for two reasons. (1) Of the studies that have reported the amount of light absorbed for their measurements of $\varphi_{PM,\lambda}$, the light absorbed is significantly higher than the maximum used in this study, implying that their $\varphi_{PM,\lambda}$ and rates of photomineralization may be even more underestimated. (2) Spectral slopes of the directly measured $\varphi_{PM,\lambda}$ that are shallower than slopes assumed from modeled $\varphi_{PM,\lambda}$ in prior studies suggest that rates of photomineralization have been underestimated in prior studies. The effect of the shallow slope of $\varphi_{PM,\lambda}$ is in addition to the average 47% underestimation from the effects of light absorption in our study. Thus, we suggest that photomineralization accounts for substantially more than the reported 10 to 30% of the total CO_2 emitted from inland surface waters to the atmosphere.[7–11]

Conflicts of interest

The authors declare no competing interests.

Data availability

All data supporting this article are available in the main text or the SI. See DOI: https://doi.org/10.1039/d5em00293a.

Acknowledgements

We thank N. LaFramboise, K. Clippinger, J. Dobkowski, N. Christman, B. Crump, E. Peterson, E. Parker, A. Malik, and researchers, technicians, and support staff of the Arctic LTER and Toolik Field Station for assistance with field and laboratory work. The research was supported by NSF DEB 1754835 and 2224743 (G. W. K. and R. M. C.), NSF DEB 1637459 and OPP 1936769 (G. W. K.), and DOE BER 273381 (R. M. C. and G. W. K.). All authors contributed to the study design, sample collection, laboratory experiments, data analysis, and manuscript preparation.

References

1 T. J. Battin, R. Lauerwald, E. S. Bernhardt, E. Bertuzzo, L. G. Gener, R. O. Hall, E. R. Hotchkiss, T. Maavara, T. M. Pavelsky, L. Ran, P. Raymond, J. A. Rosentreter and P. Regnier, River Ecosystem Metabolism and Carbon Biogeochemistry in a Changing World, *Nature*, 2023, **613**(7944), 449–459, DOI: 10.1038/s41586-022-05500-8.

2 J. J. Cole, N. F. Caraco, G. W. Kling and T. K. Kratz, Carbon Dioxide Supersaturation in the Surface Waters of Lakes, *Science*, 1994, **265**(5178), 1568–1570, DOI: 10.1126/science.265.5178.1568.

3 J. J. Cole, Y. T. Prairie, N. F. Caraco, W. H. McDowell, L. J. Tranvik, R. G. Striegl, C. M. Duarte, P. Kortelainen, J. A. Downing, J. J. Middelburg and J. Melack, Plumbing the Global Carbon Cycle: Integrating Inland Waters into the Terrestrial Carbon Budget, *Ecosystems*, 2007, **10**(1), 171–18, DOI: 10.1007/s.

4 R. H. S. Hutchins, J. P. Casas-Ruiz, Y. T. Prairie and P. A. del Giorgio, Magnitude and Drivers of Integrated Fluvial Network Greenhouse Gas Emissions across the Boreal Landscape in Québec, *Water Res.*, 2020, **173**, 115556, DOI: 10.1016/j.watres.2020.115556.

5 G. W. Kling, G. W. Kipphut and M. C. Miller, Arctic Lakes and Streams as Gas Conduits to the Atmosphere: Implications for Tundra Carbon Budgets, *Science*, 1991, **251**(4991), 298–301, DOI: 10.1126/science.251.4991.298.

6 P. A. Raymond, J. Hartmann, R. Lauerwald, S. Sobek, C. McDonald, M. Hoover, D. Butman, R. Striegl, E. Mayorga, C. Humborg, P. Kortelainen, H. Dürr, M. Meybeck, P. Ciais and P. Guth, Global Carbon Dioxide Emissions from Inland Waters, *Nature*, 2013, **503**(7476), 355–359, DOI: 10.1038/nature12760.

7 R. M. Cory, C. P. Ward, B. C. Crump and G. W. Kling, Sunlight Controls Water Column Processing of Carbon in Arctic Fresh Waters, *Science*, 2014, **345**(6199), 925–928, DOI: 10.1126/science.1253119.

8 M. Groeneveld, L. Tranvik, S. Natchimuthu and B. Koehler, Photochemical Mineralisation in a Boreal Brown Water Lake: Considerable Temporal Variability and Minor Contribution to Carbon Dioxide Production, *Biogeosciences*, 2016, **13**(13), 3931–3943, DOI: 10.5194/bg-13-3931-2016.

9 B. Koehler, E. Broman and L. J. Tranvik, Apparent Quantum Yield of Photochemical Dissolved Organic Carbon Mineralization in Lakes, *Limnol. Oceanogr.*, 2016, **61**(6), 2207–2221, DOI: 10.1002/lno.10366.

10 B. Koehler, T. Landelius, G. A. Weyhenmeyer, N. Machida and L. J. Tranvik, Sunlight-Induced Carbon Dioxide Emissions from Inland Waters, *Global Biogeochem. Cycles*, 2014, **28**, 696–711, DOI: 10.1002/2014GB004850.

11 D. Vachon, J. F. Lapierre and P. A. Del Giorgio, Seasonality of Photochemical Dissolved Organic Carbon Mineralization and Its Relative Contribution to Pelagic CO_2 Production in Northern Lakes, *J. Geophys. Res.:Biogeosci.*, 2016, **121**(3), 864–878, DOI: 10.1002/2015JG003244.

12 C. P. Ward, J. C. Bowen, D. H. Freeman and C. M. Sharpless, Rapid and Reproducible Characterization of the Wavelength Dependence of Aquatic Photochemical Reactions Using Light-Emitting Diodes, *Environ. Sci. Technol. Lett.*, 2021, **8**(5), 437–442, DOI: 10.1021/acs.estlett.1c00172.

13 S. S. Andrews, S. Caron and O. C. Zafiriou, Photochemical Oxygen Consumption in Marine Waters: A Major Sink for Colored Dissolved Organic Matter?, *Limnol. Oceanogr.*, 2000, **45**(2), 267–277, DOI: 10.4319/lo.2000.45.2.0267.

14 W. Granéli, M. Lindell, B. M. De Faria and F. D. A. Esteves, Photoproduction of Dissolved Inorganic Carbon in Temperate and Tropical Lakes - Dependence on Wavelength Band and Dissolved Organic Carbon Concentration, *Biogeochemistry*, 1998, **43**(2), 175–195, DOI: 10.1023/A:1006042629565.

15 S. C. Johannessen and W. L. Miller, Quantum Yield for the Photochemical Production of Dissolved Inorganic Carbon in Seawater, *Mar. Chem.*, 2001, **76**(4), 271–283, DOI: 10.1016/S0304-4203(01)00067-6.

16 R. M. Cory, B. C. Crump, J. A. Dobkowski and G. W. Kling, Surface Exposure to Sunlight Stimulates CO_2 Release from Permafrost Soil Carbon in the Arctic, *Proc. Natl. Acad. Sci. U. S. A.*, 2013, **110**(9), 3429–3434, DOI: 10.1073/pnas.1214104110.

17 J. C. Bowen, C. P. Ward, G. W. Kling and R. M. Cory, Arctic Amplification of Global Warming Strengthened by Sunlight Oxidation of Permafrost Carbon to CO_2, *Geophys. Res. Lett.*, 2020, **47**(12), 3, DOI: 10.1029/2020GL087085.

18 A. V. Vähätalo, M. Salkinoja-Salonen, P. Taalas and K. Salonen, Spectrum of the Quantum Yield for Photochemical Mineralization of Dissolved Organic Carbon in a Humic Lake, *Limnol. Oceanogr.*, 2000, **45**(3), 664–676, DOI: 10.4319/lo.2000.45.3.0664.

19 C. Fasching and T. J. Battin, Exposure of Dissolved Organic Matter to UV-Radiation Increases Bacterial Growth Efficiency in a Clear-Water Alpine Stream and Its Adjacent Groundwater, *Aquat. Sci.*, 2012, **74**(1), 143–153, DOI: 10.1007/s00027-011-0205-8.

20 S. E. Page, J. R. Logan, R. M. Cory and K. McNeill, Evidence for Dissolved Organic Matter as the Primary Source and Sink of Photochemically Produced Hydroxyl Radical in Arctic Surface Waters, *Environ. Sci.:Processes Impacts*, 2014, **16**(4), 807–822, DOI: 10.1039/c3em00596h.

21 M. Peterson, M. McNally, M. Cory, D. Thoemke, J. Cotner and K. McNeill, Spatial and Temporal Distribution of Singlet Oxygen in Lake Superior, *Environ. Sci. Technol.*, 2012, **46**(13), 7222–7229, DOI: 10.1021/es301105e.

22 J. Wasswa, C. T. Driscoll and T. Zeng, Photochemical Characterization of Surface Waters from Lakes in the Adirondack Region of New York, *Environ. Sci. Technol.*, 2020, **54**(17), 10654–10667, DOI: 10.1021/acs.est.0c02811.

23 S. M. Berg, K. H. Wammer and C. K. Remucal, Dissolved Organic Matter Photoreactivity Is Determined by Its Optical Properties, Redox Activity, and Molecular Composition, *Environ. Sci. Technol.*, 2023, **57**(16), 6703–6711, DOI: 10.1021/acs.est.3c01157.

24 R. P. Milstead, E. R. Horvath and C. K. Remucal, Dissolved Organic Matter Composition Determines Its Susceptibility to Complete and Partial Photooxidation within Lakes, *Environ. Sci. Technol.*, 2023, **57**(32), 11876–11885, DOI: 10.1021/acs.est.3c01500.

25 J. L. Weishaar, G. R. Aiken, B. A. Bergamaschi, M. S. Fram, R. Fujii and K. Mopper, Evaluation of Specific Ultraviolet Absorbance as an Indicator of the Chemical Composition and Reactivity of Dissolved Organic Carbon, *Environ. Sci. Technol.*, 2003, **37**(20), 4702–4708, DOI: 10.1021/es030360x.

26 R. M. Cory, D. M. McKnight, Y. P. Chin, P. Miller and C. L. Jaros, Chemical Characteristics of Fulvic Acids from Arctic Surface Waters: Microbial Contributions and

Photochemical Transformations, *J. Geophys. Res.:Biogeosci.*, 2007, **112**(4), 1–14, DOI: 10.1029/2006JG000343.

27 W. L. Miller and R. G. Zepp, Photochemical Production of Dissolved Inorganic Carbon from Terrestrial Organic Matter: Significance to the Oceanic Organic Carbon Cycle, *Geophys. Res. Lett.*, 1995, **22**(4), 417–420, DOI: 10.1029/94GL03344.

28 H. E. Reader and W. L. Miller, The Efficiency and Spectral Photon Dose Dependence of Photochemically Induced Changes to the Bioavailability of Dissolved Organic Carbon, *Limnol. Oceanogr.*, 2014, **59**(1), 182–194, DOI: 10.4319/lo.2014.59.1.0182.

29 L. C. Powers and W. L. Miller, Photochemical Production of CO and CO_2 in the Northern Gulf of Mexico: Estimates and Challenges for Quantifying the Impact of Photochemistry on Carbon Cycles, *Mar. Chem.*, 2015, **171**, 21–35, DOI: 10.1016/j.marchem.2015.02.004.

30 Y. Zhang, H. Xie and G. Chen, Factors Affecting the Efficiency of Carbon Monoxide Photoproduction in the St. Lawrence Estuarine System (Canada), *Environ. Sci. Technol.*, 2006, **40**(24), 7771–7777, DOI: 10.1021/es0615268.

31 L. C. Powers and W. L. Miller, Hydrogen Peroxide and Superoxide Photoproduction in Diverse Marine Waters: A Simple Proxy for Estimating Direct CO_2 Photochemical Fluxes, *Geophys. Res. Lett.*, 2015, **42**(18), 7696–7704, DOI: 10.1002/2015GL065669.

32 C. P. Ward and R. M. Cory, Complete and Partial Photo-Oxidation of Dissolved Organic Matter Draining Permafrost Soils, *Environ. Sci. Technol.*, 2016, **50**(7), 3545–3553, DOI: 10.1021/acs.est.5b05354.

33 A. V. Vähätalo and R. G. Wetzel, Photochemical and Microbial Decomposition of Chromophoric Dissolved Organic Matter during Long (Months-Years) Exposures, *Mar. Chem.*, 2004, **89**(1–4), 313–326, DOI: 10.1016/j.marchem.2004.03.010.

34 R. M. Cory, K. H. Harrold, B. T. Neilson and G. W. Kling, Controls on Dissolved Organic Matter (DOM) Degradation in a Headwater Stream: The Influence of Photochemical and Hydrological Conditions in Determining Light-Limitation or Substrate-Limitation of Photo-Degradation, *Biogeosciences*, 2015, **12**(22), 6669–6685, DOI: 10.5194/bg-12-6669-2015.

35 C. J. Miles and P. L. Brezonik, Oxygen Consumption in Humic-Colored Waters by a Photochemical Ferrous-Ferric Catalytic Cycle, *Environ. Sci. Technol.*, 1981, **15**(9), 1089–1095, DOI: 10.1021/es00091a010.

36 H. Xie, O. C. Zafiriou, W. J. Cai, R. G. Zepp and Y. Wang, Photooxidation and Its Effects on the Carboxyl Content of Dissolved Organic Matter in Two Coastal Rivers in the Southeastern United States, *Environ. Sci. Technol.*, 2004, **38**(15), 4113–4119, DOI: 10.1021/es035407t.

37 D. J. Kieber, G. W. Miller, J. Neale and K. Mopper, Wavelength and Temperature-Dependent Apparent Quantum Yields for Photochemical Formation of Hydrogen Peroxide in Seawater, *Environ. Sci.: Processes Impacts*, 2014, **28**(1), 777–791, DOI: 10.1039/c4em00036f.

38 A. Marchisio, M. Minella, V. Maurino, C. Minero and D. Vione, Photogeneration of Reactive Transient Species upon Irradiation of Natural Water Samples: Formation Quantum Yields in Different Spectral Intervals, and Implications for the Photochemistry of Surface Waters, *Water Res.*, 2015, **73**, 145–156, DOI: 10.1016/j.watres.2015.01.016.

39 L. C. Powers and W. L. Miller, Apparent Quantum Efficiency Spectra for Superoxide Photoproduction and Its Formation of Hydrogen Peroxide in Natural Waters, *Front. Mar. Sci.*, 2016, **3**, 1–9, DOI: 10.3389/fmars.2016.00235.

40 *Alaska's Changing Arctic: Ecological Consequences for Tundra, Streams, and Lakes*, ed.Hobbie, J. E. and Kling, G. W., Oxford University Press, New York, 1st edn, 2014.

41 R. M. Cory, K. McNeill, J. P. Cotner, A. Amado, J. M. Purcell and A. G. Marshall, Singlet Oxygen in the Coupled Photochemical and Biochemical Oxidation of Dissolved Organic Matter, *Environ. Sci. Technol.*, 2010, **44**(10), 3683–3689, DOI: 10.1021/es902989y.

42 J. R. Helms, A. Stubbins, J. D. Ritchie, E. C. Minor, D. J. Kieber and K. Mopper, Absorption spectral slopes and slope ratios as indicators of molecular weight, source, and photobleaching of chromophoric dissolved organic matter, *Limnol. Oceanogr.*, 2008, **53**(3), 955–969.

43 C. P. Ward and R. M. Cory, Assessing the Prevalence, Products, and Pathways of Dissolved Organic Matter Partial Photo-Oxidation in Arctic Surface Waters, *Environ. Sci.:Processes Impacts*, 2020, **22**(5), 1214–1223, DOI: 10.1039/c9em00504h.

44 Y. Gu, A. Lensu, S. Perämäki, A. Ojala and A. V. Vähätalo, Iron and pH Regulating the Photochemical Mineralization of Dissolved Organic Carbon, *ACS Omega*, 2017, **2**(5), 1905–1914, DOI: 10.1021/acsomega.7b00453.

45 H. Gao and R. G. Zepp, Factors Influencing Photoreactions of Dissolved Organic Matter in a Coastal River of the Southeastern United States, *Environ. Sci. Technol.*, 1998, **32**(19), 2940–2946, DOI: 10.1021/es9803660.

46 D. M. Mangiante, R. D. Schaller, P. Zarzycki, J. F. Banfield and B. Gilbert, Mechanism of Ferric Oxalate Photolysis, *ACS Earth Space Chem.*, 2017, **1**(5), 270–276, DOI: 10.1021/acsearthspacechem.7b00026.

47 W. Granéli, M. Lindell and L. Tranvik, Photo-Oxidative Production of Dissolved Inorganic Carbon in Lakes of Different Humic Content, *Limnol. Oceanogr.*, 1996, **41**(4), 698–706, DOI: 10.4319/lo.1996.41.4.0698.

48 C. L. Osburn, L. Retamal and W. F. Vincent, Photoreactivity of Chromophoric Dissolved Organic Matter Transported by the Mackenzie River to the Beaufort Sea, *Mar. Chem.*, 2009, **115**(1–2), 10–20, DOI: 10.1016/j.marchem.2009.05.003.

49 R. G. M. Spencer, A. Stubbins, P. J. Hernes, A. Baker, K. Mopper, A. K. Aufdenkampe, R. Y. Dyda, V. L. Mwamba, A. M. Mangangu, J. N. Wabakanghanzi and J. Six, Photochemical Degradation of Dissolved Organic Matter and Dissolved Lignin Phenols from the Congo River, *J. Geophys. Res.:Biogeosci.*, 2009, **114**(3), 1–12, DOI: 10.1029/2009JG000968.

50 B. W. Abbott, J. R. Larouche, J. B. Jones, B. William and A. W. Balser, Elevated Dissolved Organic Carbon Biodegradability from Thawing and Collapsing Permafrost, *J. Geophys. Res.:Biogeosci.*, 2014, **119**(10), 2049–2063, DOI: **10.1002/2014JG002678**.

51 C. P. Ward, S. G. Nalven, B. C. Crump, G. W. Kling and R. M. Cory, Photochemical Alteration of Organic Carbon Draining Permafrost Soils Shifts Microbial Metabolic Pathways and Stimulates Respiration, *Nat. Commun.*, 2017, **8**(1), 1–7, DOI: **10.1038/s41467-017-00759-2**.

52 E. M. Herndon, Z. Yang, J. Bargar, N. Janot, T. Z. Regier, D. E. Graham, S. D. Wullschleger, B. Gu and L. Liang, Geochemical Drivers of Organic Matter Decomposition in Arctic Tundra Soils, *Biogeochemistry*, 2015, **126**(3), 397–414, DOI: **10.1007/s10533-015-0165-5**.

53 A. Trusiak, L. Treibergs, G. Kling and R. Cory, The Controls of Iron and Oxygen on Hydroxyl Radical (˙OH) Production in Soils, *Soil Syst.*, 2018, **3**(1), 1, DOI: **10.3390/soilsystems3010001**.

54 A. M. Kellerman, F. Guillemette, D. C. Podgorski, G. R. Aiken, K. D. Butler and R. G. M. Spencer, Unifying Concepts Linking Dissolved Organic Matter Composition to Persistence in Aquatic Ecosystems, *Environ. Sci. Technol.*, 2018, **52**(5), 2538–2548, DOI: **10.1021/acs.est.7b05513**.

55 E. C. Rieb, C. A. Polik, C. P. Ward, G. W. Kling and R. M. Cory, Controls on the Respiration of Ancient Carbon Draining from Permafrost Soils into Sunlit Arctic Surface Waters, *J. Geophys. Res.:Biogeosci.*, 2024, **129**(5), DOI: **10.1029/2023JG007853**.

56 Y. H. Xiao, T. Sara-Aho, H. Hartikainen and A. V. Vähätalo, Contribution of Ferric Iron to Light Absorption by Chromophoric Dissolved Organic Matter, *Limnol. Oceanogr.*, 2013, **58**(2), 653–662, DOI: **10.4319/lo.2013.58.2.0653**.

57 B. T. Neilson, M. B. Cardenas, M. T. O'Connor, M. T. Rasmussen, T. V. King and G. W. Kling, Groundwater Flow and Exchange Across the Land Surface Explain Carbon Export Patterns in Continuous Permafrost Watersheds, *Geophys. Res. Lett.*, 2018, **45**(15), 7596–7605, DOI: **10.1029/2018GL078140**.

58 S. C. Whalen and J. C. Cornwell, Nitrogen, Phosphorus, and Organic Carbon Cycling in an Arctic Lake, *Can. J. Fish. Aquat. Sci.*, 1985, **42**(4), DOI: **10.1139/f85-102**.

59 A. Stubbins, P. J. Mann, L. Powers, T. B. Bittar, T. Dittmar, C. P. McIntyre, T. I. Eglinton, N. Zimov and R. G. M. Spencer, Low Photolability of Yedoma Permafrost Dissolved Organic Carbon, *J. Geophys. Res.:Biogeosci.*, 2017, **122**(1), 200–211, DOI: **10.1002/2016JG003688**.